In summary, the present work demonstrates that XPS can determine thermochemical values that are often inaccessible by any other method and provides important, new quantitative insights into the fundamental driving forces in surface and interface segregation.

---

[1] J. H. Sinfelt and J. A. Cusumano, in *Advanced Materials in Catalysis*, edited by J. J. Burton and R. L. Garten (Academic, New York, 1977), p. 1.

[2] A. Rosengren and B. Johansson, Phys. Rev. B **23**, 3852 (1981); B. Johansson and N. Mårtensson, Phys. Rev. B **21**, 4427 (1980). See also related material: P. Steiner and S. Hüfner, Solid State Commun. **37**, 279 (1981); V. Kumar, D. Tománek, and K. H. Bennemann, Solid State Commun. **39**, 987 (1981).

[3] D. A. Shirley, Chem. Phys. Lett. **16**, 220 (1972).

[4] Preliminary indications are that the accuracy attainable by this general approach to determining thermochemical values is about ±1.0 kcal/mole. See P. Steiner and S. Hüfner, Solid State Commun. **37**, 79 (1981), for the accuracy of this method in bulk Pd-Ag alloys. It must be kept in mind that the excited Ni atom and the Cu atom are equated only in the sense that they are expected to have essentially indistinguishable thermochemical properties. The excellence of this approximation when used in this manner no doubt derives from the fact that the Coulomb integral for a valence-shell electron with a core electron scarcely changes when the core-electron orbital is shrunk to a point [see J. B. Mann, Los Alamos Scientific Laboratory Report No. LA-3690, 1967 (unpublished) and Ref. 3]. A more complete analysis of the anticipated error in the equivalent-core approximation is now in progress (W. F. Egelhoff, Jr., to be published). It suggests that in Cu-Ni this error makes the measured thermochemical values about 3% too small. Thus the uncertainty will depend almost entirely on the degree to which XPS can be used to determine shifts in the binding energy of the fully screened core hole.

[5] For experimental details see W. F. Egelhoff, Jr., Appl. Surf. Sci. **11/12**, 761 (1982).

[6] W. F. Egelhoff, Jr., to be published.

[7] A. R. Miedema, Z. Metallkd. **69**, 455 (1978).

[8] In this conceptual framework, the single initial state is a Cu(100) crystal with an epitaxial Ni monolayer on it and a single Ni atom dissolved in the bulk. The two final states are produced by XPS on either a surface Ni atom or the bulk Ni atom.

[9] L. Elford, F. Muller, and O. Kubaschewski, Z. Elektrochem. **73**, 601 (1969).

[10] H. H. Brongersma, M. J. Sparnaay, and T. M. Buck, Surf. Sci. **71**, 657 (1978).

Universality in the Critical Broadening of Spectral Lines in Simple Fluids

Shaul Mukamel

Department of Chemistry, University of Rochester, Rochester, New York 14627

and

Peter S. Stern

Chemical Physics Department, Weizmann Institute of Science, Rehovot, Israel 76100

and

David Ronis

Department of Chemistry, Harvard University, Cambridge, Massachusetts 02138

Nonlinear mode-coupling hydrodynamics is used to study the broadening of spectral lines near a liquid-gas critical point. The critical contribution to the line shape is given by a universal line-shape function. For values of $\epsilon = |(T - T_c)/T_c|$ which are not too small, the line assumes a Lorentzian form and the width $\hat{\Gamma}$ increases as $\sim \epsilon^s$ with the critical exponent $s = \gamma + \nu = -0.607$. Very close to the critical point the line changes into a Levy distribution [the Fourier transform of $\exp(-t^r)$ where $r = (3 - \eta)/2$] and the line shape becomes independent of ϵ ($s = 0$).

PACS numbers: 64.70.Fx, 05.40.+j, 72.80.-e

In this work we consider the broadening of an isolated spectral line in a fluid near a critical point. Using hydrodynamic mode-coupling techniques, we derive a universal line-shape function and analyze the critical exponent associated with the line width. Our theory accounts quantitatively for the available experimental data on vibrational dephasing in N_2 and O_2.[1] A similar model was de-

veloped recently by Madden and Hills.[2] Our analysis, however, is much more general and we are able to provide a complete solution for the universal line-shape function. Consider a fluid consisting of N two-level particles with pairwise additive interactions. The ground state will be denoted by $|a\rangle$ and the excited state by $|b\rangle$. We denote the interaction of two atoms in the $|a\rangle$ state by $V_a(Q)$ and of one atom in $|a\rangle$ and another in $|b\rangle$ by $V_b(Q)$; then the interaction responsible for the line broadening is $U \equiv V_b(Q) - V_a(Q)$. Here, Q is the interatomic separation. The absorption

line shape for this system, $I(\Delta)$, may be written in the form[3]

$$I(\Delta) = \frac{1}{\pi} \operatorname{Re} \int_0^\infty d\tau \, \exp(i\Delta\tau)\exp[-\varphi(\tau)], \tag{1}$$

where

$$\varphi(\tau) \equiv \int_0^\tau d\tau_1 (\tau - \tau_1)\langle U(\tau_1)U(0)\rangle. \tag{2}$$

Here $\Delta = \omega_L - \omega_{ba}$ is the detuning of the radiation frequency ω_L from the two-level frequency ω_{ba} and $\langle U(\tau)U(0)\rangle$ is the ground-state correlation function:

$$\langle U(\tau)U(0)\rangle = \sum_{\vec{k},\vec{k}'} U_{\vec{k}}^* U_{\vec{k}'}[\langle N_{\vec{k}}(\tau)\hat{N}_{-\vec{k}}(\tau)N_{\vec{k}'}(0)\hat{N}_{-\vec{k}'}(0)\rangle - \langle N_{\vec{k}}\hat{N}_{-\vec{k}}\rangle\langle N_{\vec{k}'}\hat{N}_{-\vec{k}'}\rangle]. \tag{3}$$

$N_{\vec{k}}$ and $\hat{N}_{\vec{k}}$ are the particle number density operators of the fluid and the density of a tagged particle (the absorber), respectively;

$$N_{\vec{k}} = \sum_\alpha \exp(i\vec{k}\cdot\vec{Q}_\alpha), \tag{4a}$$

$$\hat{N}_{\vec{k}} = \exp(i\vec{k}\cdot\vec{Q}_s), \tag{4b}$$

and

$$U_{\vec{k}} = \int d^3r \, U(r)\exp(i\vec{k}\cdot\vec{r}). \tag{4c}$$

The evaluation of the line-shape function (1) involves the calculation of the four-point (three-particle, two-time) correlation function appearing in Eq. (3) and it is the critical behavior of this correlation function that is being probed by the line-broadening experiment.

Using standard correlation-function manipulations, we may write

$$\langle N_{\vec{k}}(\tau)\hat{N}_{-\vec{k}}(\tau)N_{\vec{k}'}\hat{N}_{-\vec{k}'}\rangle \equiv \langle N_{\vec{k}}\hat{N}_{-\vec{k}}\rangle\langle N_{\vec{k}'}\hat{N}_{-\vec{k}'}\rangle + \langle N_{\vec{k}}(\tau)N_{\vec{k}'}\rangle\langle\hat{N}_{-\vec{k}}(\tau)\hat{N}_{-\vec{k}'}\rangle + \langle N_{\vec{k}}(\tau)\hat{N}_{-\vec{k}'}\rangle\langle\hat{N}_{-\vec{k}}(\tau)N_{\vec{k}'}\rangle$$

$$+ \langle\langle N_{\vec{k}}(\tau)\hat{N}_{-\vec{k}}(\tau)\hat{N}_{\vec{k}'}\hat{N}_{-\vec{k}'}\rangle\rangle \equiv \mathrm{I} + \mathrm{II} + \mathrm{III} + \mathrm{IV}. \tag{5}$$

Equation (5) is merely a definition of the cumulant average $\langle\langle\cdots\rangle\rangle$. It may be easily shown that the contribution to Eq. (3) of III/II is $O(1/\Omega)$, where Ω is the volume of the system. Thus in the thermodynamic limit $(\Omega \to \infty, N \to \infty, N/\Omega = n$ finite) we may safely ignore III. We have evaluated IV using the mode-coupling theory in the bare-vertex approximation.[4,5] This results in an expression for IV involving nonlinear couplings of $N_{\vec{k}}$ and $\hat{N}_{\vec{k}}$ to shear fluctuations. The shear relaxation time is much shorter than the time scales characterizing $N_{\vec{k}}$ (heat diffusion) and $\hat{N}_{\vec{k}}$ (self-diffusion). In addition, the shear viscosity is known not to display any strong critical behavior.[5,6] These facts have allowed us to show[7] that the contribution of IV/II is $O(\xi_0/\xi) \sim O((-\epsilon)^\nu)$, where ξ_0/ξ is the ratio of a microscopic length scale to the correlation length, $\epsilon = |T - T_c|/T_c$ is the reduced temperature, and ν is the correlation-length critical exponent. It must be stressed that IV is small only near the critical point. The term I is canceled when (5) is substituted in (3). We therefore

get

$$\langle U(\tau)U(0)\rangle = U_0^2 \sum_{\vec{k}} \langle N_{\vec{k}}(\tau)N_{-\vec{k}}\rangle\langle\hat{N}_{-\vec{k}}(\tau)\hat{N}_{\vec{k}}\rangle. \tag{6}$$

In Eq. (6) we have also replaced U_k in the sum by U_0 since we are going to evaluate the sum in the long-wavelength limit. This forces us to introduce an upper cutoff, $k_c \approx 10^8$ cm^{-1}, in the sum in Eq. (6). As will become clear below [cf. Eq. (9b)], for systems with long dephasing times the cutoff is unimportant. We have calculated Eq. (6) using the following hydrodynamic expressions for the two-point correlation functions[6]:

$$\langle\hat{N}_{-\vec{k}}(\tau)\hat{N}_{\vec{k}}\rangle = \exp(-D_s k^2\tau), \tag{7a}$$

$$\Omega^{-1}\langle N_{\vec{k}}(\tau)N_{-\vec{k}}\rangle = S(k)\exp(-D_T k^2\tau). \tag{7b}$$

Here D_s is the self-diffusion coefficient, D_T is the thermal diffusivity, $S(k)$ is the static structure factor, and n is the number density in the fluid. We have used the Fisher-Burford approxi-

mant for $S(k)$ near the critical point, i.e.,[8]

$$S(k) = n \frac{\kappa_T}{\kappa_T^0} \frac{(1 + \Psi^2 k^2/\kappa^2)^{\eta/2}}{1 + (1 + \Psi^2 \eta/2)k^2/\kappa^2} . \tag{8}$$

Here κ_T/κ_T^0 is the ratio of the actual isothermal compressibility and that of an ideal gas and $\kappa = \xi^{-1}$ is the inverse of the correlation length. $\Psi = 0.075$, and $\eta = \frac{1}{18}$ is the Fisher-Burford exponent.[8] When $\Psi = \eta = 0$, Eq. (8) reduces to the Ornstein-Zernike form.[6]

The small-k picture described here is quite different from the usual collisional broadening picture of dephasing.[9] Those processes are contained in the high-k parts of the sums in Eqs. (3) and (6) and can be accounted for by convolving the line shape obtained here with the usual (and presumably noncritical, e.g., binary collision) line shape. For the systems considered here, i.e., those with long dephasing times, this will not lead to any major changes. The low-k contributions to $\varphi(\tau)$ describe the effects of fluctuations in the *mean* density on length scales large compared with that of the microscopic interaction. That is, a particle can be found in a distribution of mean density environments which can evolve in time via thermal and mass diffusion. If the latter processes are sufficiently slow compared with the inverse linewidth, then the line broadening is purely inhomogeneous. However, as we shall shortly see, this is not the case for the Raman linewidth of N_2 and O_2. Clearly as T_c is approached, the low-k fluctuations become more important and, if the high-k contributions are sufficiently small, they will dominate the line shape. Upon substitution of Eqs. (7) and (8) in Eq. (6), we finally get

$$\varphi(\tau) = AF(\Gamma \kappa^2 \tau), \tag{9}$$

where

$$A = \frac{1}{4\pi} \frac{\kappa_T}{\kappa_T^0} \frac{U_0^2 n}{\Gamma^2 \kappa} , \tag{9a}$$

$$F(x) = \frac{\sqrt{x}}{\pi} \int_0^{y_0} dy \frac{(1 + \Psi y/x)^{\eta/2}}{1 + (1 + \Psi \eta/2)y/x} \frac{\exp(-y) + y - 1}{y^{3/2}} , \tag{9b}$$

and

$$\Gamma = D_s + D_T. \tag{9c}$$

Here $y_0 = k_c(\Gamma \tau)^{1/2}$ is a high-k cutoff. Using data for N_2 at 90 K (i.e., $k_c \approx 10^8$ cm^{-1}, $\tau \approx 10^{-10}$ sec, and $\Gamma \approx 8 \times 10^{-4}$ cm^2/sec) we find that $k_c[\Gamma \tau]^{1/2} \approx 30$ which allows us to extend the limit of integration in Eq. (9b) to infinity. Physically, this is due to the fact that density fluctuations on the

scale of the microscopic interaction relax as a result of thermal and particle diffusion on a time scale which is shorter than the dephasing time.

The function $F(x)$ behaves as $\sim x^{(3-\eta)/2}$ for $x \ll 1$, and asymptotically for $x \gg 1$, $F \sim x$. A simple uniform approximation for $F(x)$ (good to within $\sim 5\%$) is

$$F(x) \cong Px^{(3-\eta)/2}/(1 + Qx^{(1-\eta)/2}), \tag{10}$$

where $P = 0.715$ and $Q = 0.706$; consequently we have

$$\exp[-\varphi(\tau)] \simeq \begin{cases} \exp[-(P/Q)A\Gamma\kappa^2\tau], & A \lesssim 10^{-2} \\ \exp[-AP(\Gamma\kappa^2\tau)^{(3-\eta)/2}], & A \gtrsim 10^2. \end{cases} \tag{11}$$

Therefore, for small A, $A < 10^{-2}$, the line shape assumes a Lorentzian form with full width at half maximum (FWHM) $\hat{\Gamma} = 2 PA\Gamma\kappa^2/Q$. For $A > 10^2$, the line assumes the form of a Levy distribution[10] with the width $\hat{\Gamma} \sim (AP)^{2/(3-\eta)}\Gamma\kappa^2$. We have calculated the line shapes using Eqs. (1) and (9b) and in Fig. 1 we display $\log\hat{\Gamma}$ vs $\log A$. We note that as predicted from the above analysis the slope of the curve changes from 1 for $A < 10^{-2}$ to $2/(3 - \eta)$ for $A > 10^2$. In order to analyze the critical behavior of our line shape let us recall the critical behavior[6] of the various parameters which appear in Eq. (9):

$$\kappa = \kappa_0 \epsilon^\nu, \quad \kappa_T/\kappa_T^0 \approx \frac{4}{9} \epsilon^{-\gamma},$$

where the factor of $\frac{4}{9}$ is obtained from the van der Waals equation of state,

$$D_s \simeq kT\kappa_0/6\pi\bar{\eta} \sim \epsilon^0, \quad D_T \simeq kT\kappa/6\pi\bar{\eta} \sim \epsilon^\nu.$$

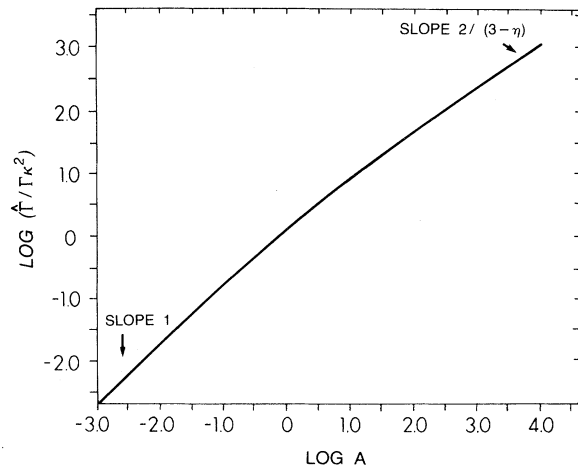FIG. 1. Universal behavior of the dimensionless linewidth $(\hat{\Gamma}/\Gamma\kappa^2)$ vs A. Note how the slope gradually changes from 1 for small A to $2/(3 - \eta)$ for large A. The line shapes were calculated using Eqs. (1) and (9).

Here κ_0^{-1} is a microscopic length ~ 1 Å and $\bar{\eta}$ is the viscosity. The critical exponents ν and γ are $\nu = \frac{9}{14}$ and $\gamma = 1.25$. Using Eq. (9) we get the critical behavior of our line-shape parameters:

$$A = A_0 \epsilon^{-\gamma - \nu}, \tag{12a}$$

$$A_0 = (9\pi)^{-1} U_0^2 n / \Gamma^2 \kappa_0, \tag{12b}$$

$$\Gamma = D_T + D_s \sim \epsilon^0. \tag{13}$$

Using Eq. (11), we immediately get, for the FWHM $\hat{\Gamma}$ of our line-shape function, $\hat{\Gamma} \sim \epsilon^s$, where

$$s = \begin{cases} -\gamma + \nu = -0.607, & A \leqslant 10^{-2} \\ -2[\gamma - \nu(2-\eta)]/(3-\eta) = 0, & A \geqslant 10^2. \end{cases} \tag{14}$$

In Eq. (13), we have assumed that we are close enough to the critical point so that $D_T \ll D_s$. Should the reverse be true, then $\Gamma \sim \epsilon^\nu$ and the slope s in the $A \leqslant 10^{-2}$ case will change to $s = -\gamma = -1.25$. The vanishing of s for $A \geqslant 10^2$ arises from the scaling identity[6] $\gamma = \nu\,(2 - \eta)$. In Fig. 2 we display $\log\hat{\Gamma}$ vs $\log\epsilon$ for various values of A_0. All the information necessary for Fig. 2 is contained in Fig. 1 together with Eq. (12a). We note that the slope gradually changes from -0.607 to 0 but the value of ϵ for which the crossover occurs depends on the value of A_0. The experimental data for O_2 and N_2 are also displayed in Fig. 2 and the fit is very good with $A_0 = 7.5 \times 10^{-4}$ and 2.5×10^{-4}, respectively. The value of A_0 obtained here agrees very nicely with the ordinary (non-critical) data for liquid N_2.[11] We note that away from the critical point $\tau_c = (\Gamma \kappa_0^2)^{-1}$ is a duration of a collision and $\langle U^2 \rangle = U_0^2 n / \kappa_0^3$ is the ensemble average for U_0^2 (n/κ_0^3 is the mean number of perturbers in the interaction region and U_0^2 is the interaction per perturber). We therefore have $A_0 \sim \langle U^2 \rangle \tau_c^2$. The latter quantity was evaluated by Oxtoby[11] for liquid N_2 and found to be $\sim 10^{-3}$, which is in good agreement with our fit. We should further note that $\langle U^2 \rangle$ (and A_0) may be alternatively estimated from purely macroscopic considerations by looking at the density dependence of the level shift $\langle U^2 \rangle \sim (\partial\bar{\omega}/\partial n)^2$, $\bar{\omega}$ being the mean frequency of the line shape and n being the density. This may give another independent estimate for A_0 using experimental data which may be readily available. This estimate is not perturbative in the intermolecular forces [unlike Eq. (2)]. Finally, the present formulation may be extended to other relaxation phenomena such as T_1 without major difficulty.

We thank D. Chandler for useful discussions. Acknowledgement is made to the donors of the
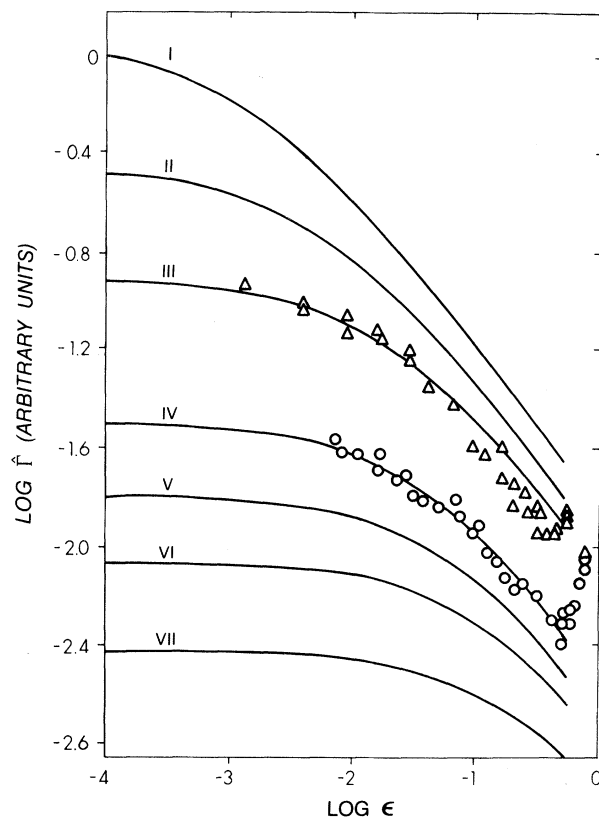

FIG. 2. Linewidth $\hat{\Gamma}$ vs ϵ for various values of A_0. In all cases the slope changes from -0.607 for large ϵ to 0 for small ϵ. The various curves were shifted arbitrarily in the vertical direction for clarity in the presentation. The points are the experimental data of Clouter and Kiefte (Ref. 1) on vibrational Raman linewidth in O_2 (circles) and N_2(triangles). I, $A_0 = 2.5 \times 10^{-6}$; II, $A_0 = 2.5 \times 10^{-5}$; III, $A_0 = 2.5 \times 10^{-4}$; IV, $A_0 = 7.5 \times 10^{-4}$; V, $A_0 = 2.5 \times 10^{-3}$; VI, $A_0 = 7.5 \times 10^{-3}$; VII, $A_0 = 2.5 \times 10^{-2}$.

[1]M. J. Clouter and H. Kiefte, J. Chem. Phys. 66, 1736 (1977).
[2]B. P. Hills and P. A. Madden, Mol. Phys. 37, 937 (1979).
[3]S. Mukamel, Phys. Rev. A 26, 617 (1982); S. Mukamel and D. Grimbert, J. Chem. Phys. 76, 834 (1982).
[4]D. Ronis, Physica (Utrecht) 167A, 25 (1981).
[5]K. Kawasaki, Ann. Phys. (N.Y.) 61, 1 (1970).
[6]E. H. Stanley, Introduction to Phase Transitions and Critical Phenomena (Clarendon, Oxford, 1971).

[7]S. Mukamel and D. Ronis, to be published.

[8]M. F. Fisher and R. J. Burford, Phys. Rev. 156, 583 (1967); R. F. Chang, H. Burstyn, and J. V. Sengers, Phys. Rev. A 19, 866 (1979).

[9]P. W. Anderson, Phys. Rev. 86, 809 (1952).

[10]W. Feller, An Introduction to Probability Theory and Its Applications (Wiley, New York, 1966), Vol. 1; B. D. Hughes, M. F. Schlesinger and F. W. Montroll, Proc. Natl. Acad. Sci. USA 78, 3287 (1981).

[11]W. Oxtoby, Adv. Chem. Phys. 40, 1 (1979).

Light Scattering above the Nematic-to-Smectic-C Transition

S. Witanachchi, J. Huang, and J. T. Ho

Department of Physics and Astronomy, State University of New York at Buffalo, Amherst, New York 14260

(Received 13 October 1982)

The behavior of the bend elastic constant above the nematic–to–smectic-C transition in $\overline{7}S5$ is found to follow the prediction of Chen and Lubensky. The nature of the director fluctuations in $\overline{7}S5$-$\overline{8}S5$ mixtures indicates that the nematic–to–smectic-C transition near the nematic–smectic-A–smectic-C multicritical point exhibits both smectic layer and tilt fluctuations and is not adequately described by existing models.

The nematic–to–smectic-A (NA) transition has been studied extensively.[1] The nematic–to–smectic-C (NC) transition, on the other hand, has received less attention. One interesting aspect of the NC transition which has remained unresolved is the critical behavior of the Frank elastic constants. Using an infinite-dimensional density wave order parameter, de Gennes suggested that all three Frank elastic constants should diverge as $\xi^{3/2}$, where ξ is the smectic correlation length.[2] Starting from a similar point of view but describing the NA and NC transitions in the same model with different free-energy parameters, Chen and Lubensky predicted a ξ^2 divergence.[3] Finally, with an additional dipolar order parameter, Chu and McMillan predicted a divergence proportional to ξ.[4] Experimentally, the only quantitative attempt has been a measurement of the cholesteric pitch near the smectic-C phase, which proved to be inconclusive because of the large background contribution.[5] Another phenomenon which is not well understood is the nature of the nematic–smectic-A–smectic-C (NAC) multicritical point, which occurs when a material with an NC transition is mixed with another with an NA and a smectic-A–to–smectic-C (AC) transition.[6] This has been the subject of several theoretical[3,4,7-9] and experimental[10-12] studies. None of the suggested models describes satisfactorily the observed behavior near the NAC point. We report here the results of light-scattering studies above the NC transition in 4-n-pentyl-phenylthiol-4′-heptyloxybenzoate ($\overline{7}S5$) and its mixtures with

the octyloxy analog ($\overline{8}S5$). Our objectives are to test the validity of the various models describing the NC transition and to provide information about the nature of the director fluctuations near the NAC point.

Our samples were synthesized by M. E. Neubert of Kent State University. Pure $\overline{7}S5$ has a first-order monotropic NC transition. With the addition of $\overline{8}S5$, which exhibits second-order NA and AC transitions, the phase diagram as a function of the mole concentration x of $\overline{7}S5$ is shown in Fig. 1. The NC transition entropy decreases from $0.84R_0$ at $x = 1$ to 0 at the multicritical concentration $x_{NAC} = 0.42$.[10]

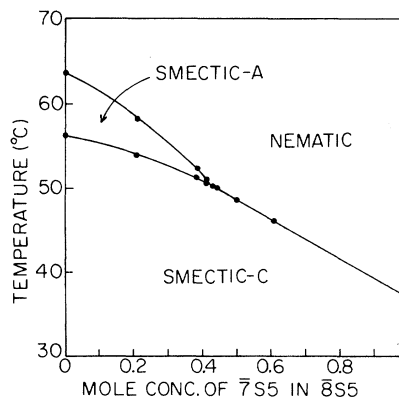Planar samples were formed between glass slides with the director parallel to the slides.

FIG. 1. Phase diagram of the $\overline{7}S5$-$\overline{8}S5$ mixtures studied.